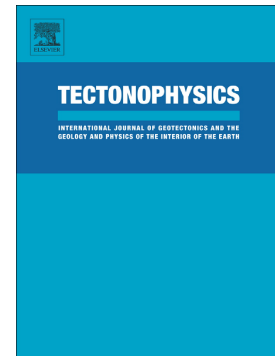


## Journal Pre-proof

Methoni Mw 6.8 rupture and aftershocks distribution from a dense array of OBS and land seismometers, offshore SW Hellenic subduction

Maria Sachpazi, Vasilis Kapetanidis, Marinos Charalampakis, Mireille Laigle, Edi Kissling, Anna Fokaefs, Elena Daskalaki, Ernst Flueh, Alfred Hirn



PII: S0040-1951(20)30326-7

DOI: <https://doi.org/10.1016/j.tecto.2020.228643>

Reference: TECTO 228643

To appear in: *Tectonophysics*

Received date: 28 April 2020

Revised date: 8 September 2020

Accepted date: 7 October 2020

Please cite this article as: M. Sachpazi, V. Kapetanidis, M. Charalampakis, et al., Methoni Mw 6.8 rupture and aftershocks distribution from a dense array of OBS and land seismometers, offshore SW Hellenic subduction, *Tectonophysics* (2020), <https://doi.org/10.1016/j.tecto.2020.228643>

This is a PDF file of an article that has undergone enhancements after acceptance, such as the addition of a cover page and metadata, and formatting for readability, but it is not yet the definitive version of record. This version will undergo additional copyediting, typesetting and review before it is published in its final form, but we are providing this version to give early visibility of the article. Please note that, during the production process, errors may be discovered which could affect the content, and all legal disclaimers that apply to the journal pertain.

Methoni Mw 6.8 rupture and aftershocks distribution from a dense array of OBS and land seismometers, offshore SW Hellenic subduction.

Maria Sachpazi<sup>a\*</sup>, Vasilis Kapetanidis<sup>b</sup>, Marinou Charalampakis<sup>a</sup>, Mireille Laigle<sup>c</sup>, Edi Kissling<sup>d</sup>, Anna Fokaefs<sup>a</sup>, Elena Daskalaki<sup>a</sup>, Ernst Flueh<sup>f</sup>, Alfred Hirn<sup>g</sup>

<sup>a</sup>*Institute of Geodynamics, National Observatory of Athens, Athens, Greece,*

<sup>b</sup>*Department of Geophysics-Geothermics, Faculty of Geology and Geoenvironment, National and Kapodistrian University of Athens, Athens, Greece*

<sup>c</sup>*Université Nice Sophia Antipolis, CNRS, IRD, Observatoire de la Côte d'Azur, Géoazur, Valbonne, France,*

<sup>d</sup>*Institute of Geophysics, ETH Zurich, Zürich, Switzerland*

<sup>f</sup>*GEOMAR Helmholtz Centre for Ocean Research, Kiel, Germany*

<sup>g</sup>*Institut de Physique du Globe de Paris, Sorbonne Paris Cité, Paris VII – Denis Diderot University, Paris, France*

\* *Corresponding author: m.sachp@noa.gr*

## **Abstract**

Along the south-western offshore Hellenic subduction zone, the overriding Aegean upper plate above the Mediterranean oceanic lithosphere generates uncommon large earthquakes on the offshore megathrust fault. The largest subduction thrust event, for half a century, is the 14 February 2008 Methoni earthquake (Mw=6.8) that occurred offshore of the southwest coast of the Peloponnesus. We conducted micro-seismicity experiments around the rupture area and forearc domain -between Peloponnesus and Crete- using ocean bottom seismometers (OBS) jointly with land-based seismological stations. Our first experiment in 2006, had revealed an association of the Matapan Trough, a 400-km-long forearc basin with local seismicity clustering and a possible gap in activity over the later Methoni rupture area. Here we present new data of post-Methoni seismic activity, recorded during 11 months beginning in October 2008 within the period of proposed afterslip on the megathrust, by an extended and dense seismic array consisting of up to 33 OBS. A minimum 1D

velocity model was constructed for the region to provide better constraints on absolute locations and double-difference relocation was applied to produce an enhanced image of the spatial distribution of hypocenters. The high resolution earthquake locations confirm correlation of the Matapan Trough with local seismicity as a regional feature, also filling up the previously observed gap. Over the Methoni rupture area, we constrain seismicity to be located mainly within the upper plate. Hypocenters are also resolved above the updip and downdip edges of the rupture area, respectively. Seismic activity provides hints of upper plate structures which were activated in response to post-seismic deformation spreading within the forearc crust. Our findings highlight the characteristics of a megathrust domain which is related with a highly deformable overriding plate and controlled by a segmented lower plate topography.

**Keywords:** Methoni earthquake, SW Hellenic subduction, aftershocks, afterslip, upper plate deformation.

## 1. Introduction

The southwestern offshore megathrust domain of the Hellenic subduction has hosted the largest earthquake of the Mediterranean area, a magnitude 8-8.5 tsunamigenic event in 365 AD (Papazachos and Papazachou, 2003; Stiros and Papageorgiou, 2001). Yet, only five interplate events with moderate magnitudes (~6.5-7.0) occurred during the instrumental period (1965-present) (Fig.1a), and only three such events occurred during the earlier period in the 19<sup>th</sup> to early 20<sup>th</sup> century (Papazachos and Papazachou, 2003).

On 14 February 2008, a  $M_w=6.8$  subduction thrust event occurred, 50 km offshore of the southwest coast of the Peloponnese, known as the Methoni earthquake (Fig.1a). Despite its moderate magnitude, it is the largest event, for half a century, in the 400 km long part of the Hellenic subduction, from the Cephalonia Transform Fault (CTF) to Crete. The Methoni event ruptured a ~ 30 km x 30 km thrust area along the plate interface between the southwestward overriding Aegean plate and the Ionian oceanic crust (Roumelioti et al., 2009). Geodetic measurements (continuous GPS time series) have shown that post-seismic slip continued for ~3 years and the total displacement is of comparable magnitude as co-seismic slip (Howell et al., 2017a). The post-seismic displacements are

attributed to afterslip on the subduction interface, distributed over a 100kmX120 km wide region including the co-seismic rupture with its greatest values observed where elevated levels of seismicity were detected following the earthquake (Howell et al., 2017a) (Fig.1b).

Afterslip occurs as a widespread post seismic process in subduction zones, complementary to the large coseismic slip zone (e.g. Cattania et al 2015; Yagi et al., 2003; Ozawa et al., 2012) and it is considered as playing an important role in promoting aftershock earthquakes on the subduction interface (Hsu et al., 2006) and the upper plate as well (Hayes et al., 2014a).

In this paper, we present observations collected from 9 to 21 months after the Methoni earthquake by a dense array of Ocean Bottom Seismometers (OBS) and seismic stations in the close onshore. We investigate post-Methoni seismicity with respect to the shape and extension of the rupture area as well as the widely distributed post seismic deformation. We combine seismic activity, focal mechanisms and structural data to characterize the pre-, co- and post-seismic behavior of the megathrust boundary over the Methoni rupture area, as well as the regional seismicity.

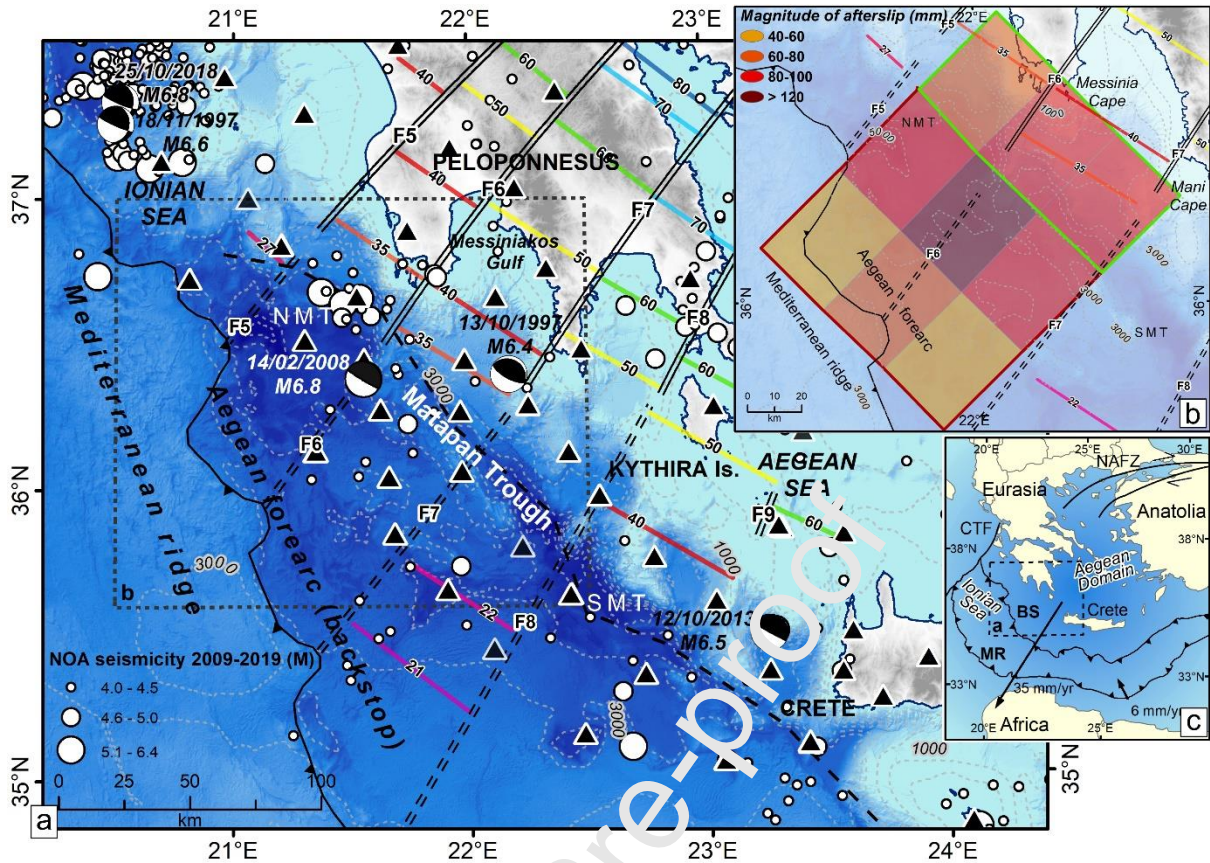


Fig.1. SW Hellenic subduction region. Background bathymetric data, here and in subsequent figures are from Brosolo et al., 2012 and Vitard et al., 2015. (a) Black triangles: the onshore-and offshore seismological stations of the Thales West Right “TWR” project. The 14 February 2008 Mw 6.8 Methoni earthquake location (indicated by its CMT Harvard focal mechanism beachball) is from Sachpazi et al. (2016b). Focal mechanisms for subduction thrust events of Mw 6.0 or greater during the instrumental period are from the CMT Harvard catalogue, except for the Crete 2013 event (Howell et al., 2017a). Earthquake locations of these events are from the National Observatory of Athens (NOA) catalogue. Here and in subsequent figures: Double-lines: Slab along-dip faults from Sachpazi et al. (2016a), labelled F5 to F9. Dashed double lines: offshore extensions of mapped onshore slab faults from Sachpazi et al. (2016b). Colored lines: isobaths of slab Moho with depth denoted in kilometres (Sachpazi et al., 2016a,b). NMT and SMT: the Northern and Southern Matapan Trough. Black barbed line: outer limit of backstop, thrust contact of the accretionary wedge of the Mediterranean Ridge over it. Black dashed NW-SE trending line: Inner limit of the backstop at the transition between the Matapan Trough to the SW and the Hellenic continental margin to the NE from

Le Pichon et al. (2019). (b) Distribution of post-seismic slip over the offshore forearc as afterslip according to geodetic data modeling (Howell et al., 2017a) with the higher  $>0.2$  resolution area marked by a green rectangle. (c) Sketch of the Hellenic subduction zone in the wider East Mediterranean context with GPS-derived velocities with respect to Eurasia (Kahle et al., 2000). Black barbed lines with triangles pointing towards opposite directions represent the external limit of the Mediterranean Ridge (MR) over the Ionian oceanic basin and the outer limit of the backstop (BS) from SW to NE respectively.

## 2. Geodynamical background and previous studies

The Hellenic subduction zone is marked in the southwestern part by subduction of the oldest oceanic lithosphere of the Mediterranean/Ionian Sea, at the edge of the African plate and the southwestwards fast advancing of the Aegean continental domain ( $\sim 4\text{cm/yr}$ ) (Kahle et al., 2000; Nocquet 2012) (Fig.1c). The Africa/Europe convergence vector is highly oblique to the margin and responsible for strain partitioning at the backstop edge (Chamot-Rooke et al., 2005).

Seismic coupling in this region has been questioned since the mid-1970s, with numerous studies concluding that the plate interface accommodates up to 80% of the convergence through aseismic slip (North, 1974; Jackson and McKenzie, 1988a,b; Baker et al., 1997; Shaw and Jackson, 2008; Shaw et al., 2010; Reilinger et al., 2010; England et al., 2016), with earthquakes of  $M_w \sim 7$  rupturing isolated locked patches (Howell et al., 2017a; Vernant et al., 2014). However, in the absence of offshore geodetic observations the size and location of these locked patches are poorly constrained. Furthermore, local offshore seismicity is not sufficiently constrained by land-based permanent stations to provide insight on the seismogenic patterns of the interplate thrust boundary or a robust and well constrained velocity model for the area.

Local scale earthquake studies on the island of Crete with onshore seismological stations provided constraints on the distribution of seismic activity associated with the subduction beneath southern Crete (Meier et al., 2004). For the region offshore southwest Crete and the southern Peloponnese however, hypocenters lack offshore constraints. A year and half before the 2008 Methoni earthquake, in May-October 2006, we conducted a pilot study over that offshore domain by deploying 5 OBS



jointly with coastal stations in order to better constrain the seismicity location. That study has revealed that the recorded hypocenters along the 250-km- long segment of the southwest Hellenic subduction zone occur mostly at 10–15 km depth, in the upper plate's crust (Sachpazi et al., 2016b). This first well-constrained local seismic activity was shown to correlate with an Aegean fore-arc specific feature, the Matapan Trough (MT) which has not previously been considered as a seismically active region.

This major ~400 km long- linear depression, reaching the greatest water depth (5km) for the Mediterranean Sea, has long been considered as the Hellenic plate boundary trench (e.g., Jongsma, 1977) and is still called the Hellenic Trench. It is a 4-5 km deep forearc basin which marks the transition between the inner forearc to the NE and the backstop to the SW (Le Pichon et al., 2019, Part 2) (Fig.1a). Despite marine seismic studies, the tectonic origin of this bathymetric feature of the Aegean plate remains controversial. Once the Mediterranean Ridge was recognized as an accretionary prism (Le Pichon et al., 1982), Huchon et al. (1982) and Le Pichon et al. (1982) interpreted the Matapan Trough as a narrow deep forearc basin. Based on Sea-Beam data and early seismic profiles, Lallemand et al. (1994) proposed that the MT is dominated by the along-arc extension. Based on seismic velocities and structure, and estimated time evolution of the Hellenic subduction zone, Le Pichon and Lallemand (2002) proposed that the backstop consists of a pile of Hellenic nappes. Shaw et al., 2010 considered instead the scarp of the Matapan Trough as the trenchward edge of the backstop to the deformed accretionary prism. This scarp would be the surface expression of a reverse fault, splaying off the deeper underlying thrust interface of the subduction zone. The authors propose that this fault, rather than the seismically low coupled plate interface, would be the causative fault that hosted the 365 AD  $M_w=8-8.5$  tsunamigenic mega-event.

The few low-angle thrust events of the instrumental period highlighting the seismogenic portion of the mega-thrust subduction fault occurred mainly arcward of the Matapan Trough (Laigle et al., 2004; Shaw et al., 2010). Even though the seismogenic interplate boundary lies offshore and is accessible by seismic reflection profiling, its imaging was hindered by its significant depth (over 15 km), the presence of the sub-surface evaporites (Chaumillon et al., 1996 ; Reston et al., 2002b) plus the stacked alpine nappes of the upper plate's crust (Le Pichon and Lallemand, 2002).

Teleseismic receiver function (RF) imaging on a dense 2D seismic array has revealed the Moho of the subducting plate, below the onshore forearc, to exhibit along-strike steps (Sachpazi et al., 2016a). The authors showed that the slab is segmented into subducting panels by a series of nine along-dip faults. Extending the imaging further offshore by 5 OBS, Sachpazi et al. (2016b) proposed that segmentation continues below the 8-10 km thick backstop to its outer limit (Fig.1a). They further suggested that these faults control the size and location of earthquakes in the megathrust boundary, such as the Methoni earthquake. This event was recorded by a nearby dense land network (Thales Was Right “TWR” Experiment) and hence could be located with the highest resolution ever obtained in that area for an event of this order of magnitude (Sachpazi et al., 2016b). The Methoni earthquake was initiated along the offshore prolongation of the intra-slab fault F6 (Fig.1a). Its focal mechanism shows a typical subduction thrust event on a N35°E dipping plane.

The source process, studied by teleseismic and regional broad band waveform modeling (Roumelioti et al., 2009), showed that the rupture extended unilaterally towards the SE along the ~2/3 of the F6F7 panel, in two areas of high coseismic slip (Fig.2a). Two hours after the mainshock, a large interplate event ( $M_w=6.5$ ) occurred at the southeastern border of the main rupture's slip extent. One week later, another strong event ( $M_w=5.9$ ) occurred in the overriding plate directly above the  $M_w=6.5$  hypocenter with a strike slip mechanism. Significant aftershock activity continued within the overriding plate over the next four months, but was manifested as a series of reverse faulting earthquakes ( $M_w$  between 4.6 and 5.4) (Fig.2a). Their hypocenters were located across the remaining eastern part of the F6F7 panel which has not slipped co-seismically. On the other hand, no such significant aftershock activity occurred at the western part of the panel. The pronounced effect of this strong activity on seismicity rate is visible as the large first peak in Fig.2b. After a relatively quiet 3-months period, two bursts of activity mark the 2<sup>nd</sup> phase of earthquake clustering and seismicity rate increase which corresponds to the observations discussed in this paper.



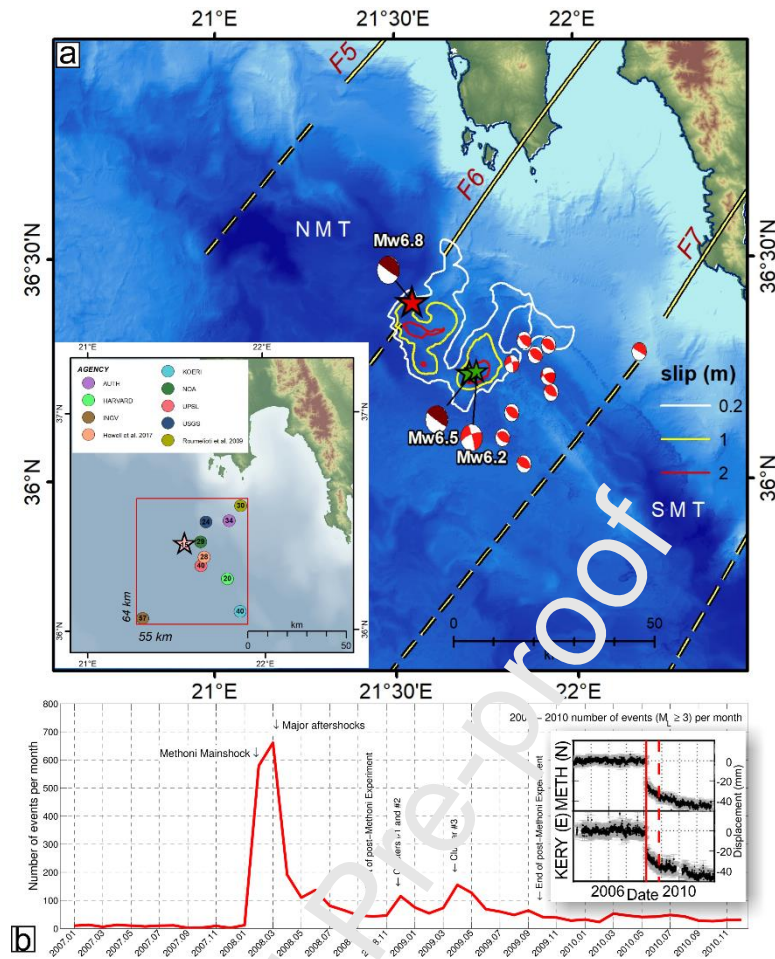


Fig. 2. Overview of the 14 February 2006 Methoni earthquake sequence and slip history. (a) Coseismic slip distribution area of the Mw=6.8 mainshock after Roumelioti et al. (2009) with the epicenters of the mainshock and stronger aftershocks  $4.5 \leq M_w \leq 6.5$  (February to June 2008) from Sachpazi et al. (2016b). The mainshock, the Mw=6.5 interplate aftershock and the Mw=6.2 shallow aftershock locations are represented by stars. CMT (Harvard) focal solutions of the mainshock and the Mw=6.5 aftershock are drawn with dark red beachballs placed in the position of the epicenters while other significant aftershocks are colored in light red. Inset map: Comparative map of the Methoni hypocenter locations by various agencies (circles) and by Sachpazi et al. (2016b), (star) with focal depths (in km) denoted by numbers inside the respective symbols. (b) Monthly seismicity rate of the area of Fig.2a, from NOA earthquake catalogue during 1 year before and 3 years after the Methoni earthquake occurrence ( $3 \leq M \leq 6.8$ ). Panel to the right side of b) shows GPS time series of stations METH and KERY (north -N- and east-E- component, respectively) from Howell et al. (2017a). The date of the start of our post-Methoni experiment is marked by dashed red line.

### 3. Data and Method

We deployed a total of 33 three-component ocean bottom seismometers (OBS) in the southwestern part of the Hellenic subduction zone, during a period of over 11 months, (October 2008-September 2009) (Fig.1a). The OBS array was complemented by 15 onshore instruments. We refer to this campaign as the “post-Methoni experiment”, and to previous experiment (May 2006-October 2006) as the “pre-Methoni experiment”. Both campaigns were part of a major onshore/offshore experiment (“TWR” EU project 2006-2011), which also involved the collection of teleseismic data used for receiver function studies across the Peloponnese (Sachpazi et al., 2016a) and its adjacent offshore domain (Sachpazi et al., 2016b). Observations from more than 2000 events were manually picked and the hypocenters were initially located using a simple 3-layer velocity model (Sachpazi et al., 2016b) and the Hypo71 code (Lee & Valdes, 1989). To improve locations, we constructed a minimum 1D P-wave velocity model using the VELEST code (Kissling, 1995; Kissling et al., 1994), which jointly inverts for the velocity model along with the respective station delays and hypocenter coordinates using a damped least squares iterative inversion scheme. The procedure was performed on a selected dataset of 1104 well-locatable events with at least 7 P-observations and azimuthal gap  $<180^\circ$ . There are many fewer events with enough S-wave picks and small gap (146 events with at least 5 P- and 5 S-wave picks on common stations, with gap  $<180^\circ$ ) and their seismic ray coverage is very sparse over most of the study area. We regarded this S data set as too small and not adequate to allow the independent construction of an 1D velocity model for S-waves. The procedure of converging towards the final 1D P-velocity model with minimum RMS error, including a series of tests to assess the stability of the produced hypocentral solutions are analytically described in Section 1 of the supplementary material.

Our final 1D P-wave velocity model (Table 1) has a fairly constant velocity in the uppermost 28km of the overriding crust (probably mixture of mostly upper continental crustal material with some underplated material). Below that depth, the effect of the 2D dipping plate interface and the oceanic Moho becomes apparent. A more pronounced step in the velocity depth function would be

expected if, across the study region, there was a Moho with some limited topography, appearing roughly sub-horizontal on a regional scale, and well sampled by the available data. On the other hand, if there is a consistently dipping Moho interface with limited 3D topography, the velocity variation from normal crustal velocities to typical mantle velocities is expected to be spread across a depth range more widely than typical for a Moho. Our final model supports the latter case for the geometries in the study region.

We further reduce the relative location uncertainties in the post-Methoni 2008-2009 seismicity by applying a double-difference relocation procedure. We incorporate the hypocenters and corrected travel-times from the results of the minimum 1D model along with differential travel-times from waveform cross-correlations (see supplementary material for a detailed description of the procedure).

Finally, we have taken advantage of the newly constructed 1D velocity model, including station-corrections, where available, to relocate the pre-Methoni 2005 sequence as well, in order to discuss the results in conjunction with the relocated catalogue of the 2008-2009 experiment. The hypocentral location of the 2008 Methoni mainshock and major aftershocks are also revisited, in light of the new velocity model.

Table 1: Final 1D P-wave velocity model for the study region. Note the typical continental crustal velocities down to 28 km. Between that depth value and 43 km depth we obtain a velocity gradient reflecting the spatial variation of the depth of the Moho, which is dipping under the area (see text).

<b>Depth (km)</b>	<b>V<sub>p</sub> (km/s)</b>
-3.0	5.80
5.0	5.90
10.0	5.92
15.0	6.26
21.0	6.29
28.0	6.93
35.0	7.27

43.0	7.95
51.0	8.00
75.0	8.10
105.0	8.20

#### 4. Results

##### *Hypocenter Locations of the pre-Methoni and post-Methoni seismicity*

Post-Methoni seismic activity is observed along the strike of the subduction zone (WNW-ESE) for over 300 km, from west of the Peloponnese up to the south-western coast of Crete (Fig.3a). Most of the seismicity is localized within a 10-30 km wide band beneath the Matapan Trough (MT) region. A similar pattern was observed for the pre-Methoni period (Fig. 3b). To the SE, along the deepest part of the MT, earthquakes are distributed along both sides of the depression, with most events remaining along its southern border. Towards Crete, seismicity is more scattered and the seismic rate is comparable during the time of the two experiments.

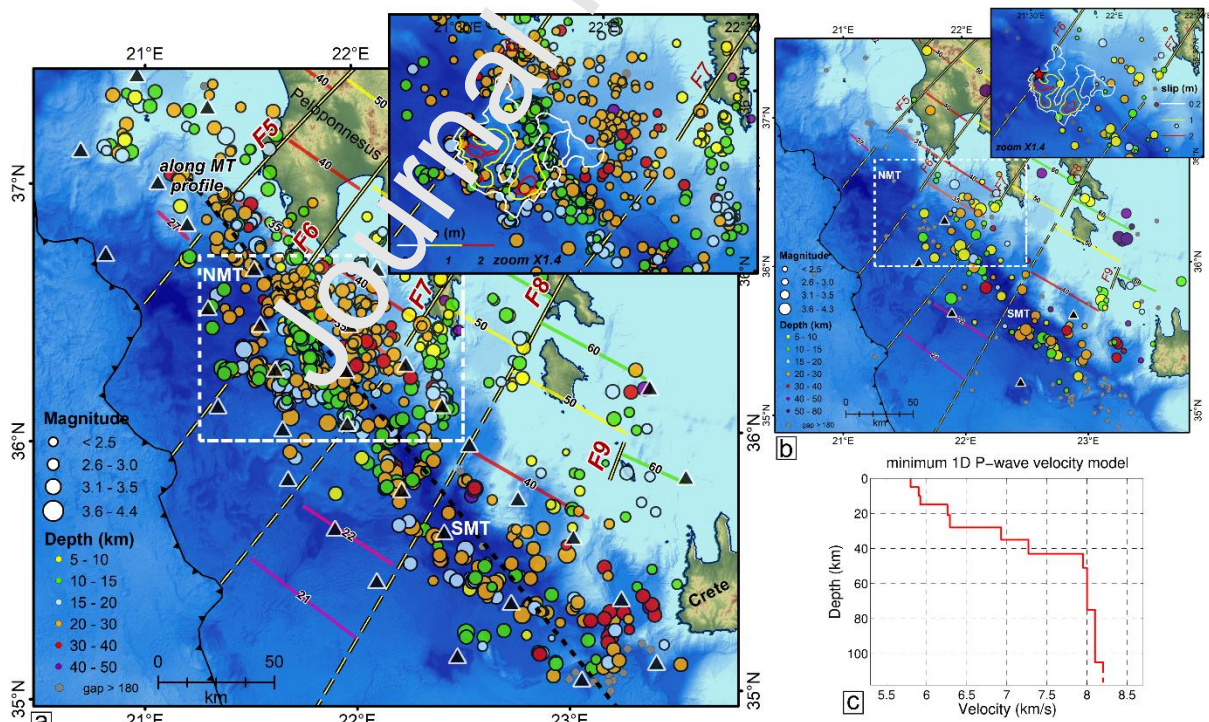


Fig. 3. Map view of seismic activity beneath the offshore forearc domain of the (a) post and (b) pre-Methoni experiments. Earthquakes of both periods are located using the plotted (c) minimum 1D P-

wave velocity model determined by the present study. The epicenters are marked by circles, scaled by their magnitude with events with azimuthal gap  $<180^\circ$  color-coded according to their focal depth (gray ones have gap  $>180^\circ$ ). The black dashed line drawn in the along-Matapan NW-SE direction in panel (a) is used for the cross-section of Fig.A.1c. Inset maps: a zoomed view of panel F6F7, marked by a white dashed rectangle in the main figures. Methoni coseismic slip is superposed while the star denotes the epicenter of Methoni earthquake.

Post-Methoni Sseismic activity is more sustained along the panel F6F7, especially in its northwestern part (Fig.3a Inset). This contrasts with the pre-Methoni period when the Methoni coseismic slip area is nearly devoid of seismic activity (Fig.3b). The quiescent area includes the part of fault F6 where the mainshock initiated. Instead, the fault is very active downdip of the rupture extent, with a large number of earthquakes located along this structure. To the SW, a stripe of earthquakes striking WNW is located along the updip border of the rupture (Fig.3a).

Integration of the existing information on the plate interface depth and geometry enables the characterization of the hypocenters with respect to the two plates. We hereafter focus on panel F6F7 which hosted the Methoni earthquake. Reflection imaging provides constraints on the depth of the slab Moho downdip the rupture (Sachpazi et al., 2016 a,b). However, the depth of the plate interface further updip, hence along the coseismic domain is unknown. Hypocentral locations of subduction thrust earthquakes such as the Methoni event may potentially provide a first order estimate of the depth of the interplate boundary. However in the present case reported hypocenters, are based mainly on distant observations, and spread over more than 40 km both horizontally and in depth (Fig.2a Inset map).

Sachpazi et al. (2016b), used phase-arrival data from the TWR land array, in addition to permanent stations, to determine hypocentral locations for the Methoni mainshock and its largest aftershocks by a simple 3-layer model with  $V_p/V_s=1.75$ . This resulted in a focal depth of 15km for the mainshock, which the authors proposed as the plate interface depth. We re-examine the mainshock's hypocentral location, using the 1D P-wave velocity model obtained from this study. For the construction of the minimum 1D  $V_p$  model, besides OBS, we have also employed data from land-based stations (see Fig.



B.1 in the supplementary material). Many of these have available data for the 2008 mainshock. The main reason the focal depth for this earthquake is so unstable is due to the fact that there were no local stations (OBS) at that time and there are significant azimuthal gaps. Thus, the trade-off between the hypocentral and velocity model parameters results in unrealistically small RMS and uncertainty estimates. In this study, we investigate the resulting range of focal depths for the mainshock by changing the only parameters for which we have control, i.e. the velocity model and distance weighting. In contrast to the seismicity of the post-Methoni experiment which was located using only P-wave data and the minimum 1-D Vp model, in the case of the mainshock we also employ a constant Vp/Vs ratio, in order to take advantage of the available S-wave arrivals, and examine how different Vp/Vs values affect the RMS error and the resulting depth. We take all these parameters into account to estimate a possible range for the focal depth of the mainshock. The resulting focal depth for the mainshock ranges from 26.5 km to 31.0 km, depending mainly on the selection of Vp/Vs and the incorporation of distant stations. We obtained lower RMS values (0.27-0.28s) when limiting the distance weighting to 50-200km. Vp/Vs=1.53 yields the smallest RMS=0.27s which is also the value supported by the Chatelain (1978) diagram for the available 2008-2009 OBS data, resulting in a focal depth of 27 km for the mainshock. Additional tests of single-event location of the 2008 mainshock with VELEST, with or without taking into account S-wave arrivals, resulted in greater focal depths (30.5-32.0km), but the RMS was also higher (0.42-0.45s). The epicentral location of the mainshock does not vary significantly in the various tests. It is clear that these various tests do not provide a way to control quantitatively the hypocenter, however, the 1D P-wave velocity model of this study is an improvement over the crude 3-layer model that was used before (model Y in Fig. B.3a in the supplementary material). Note that all the starting models (including Model Y) follow a roughly similar profile with depth (Fig. B.3a). However, starting model Y yielded the worst results (Fig. B.2, test Y2DS3). Following the above mentioned estimates we adopt a mean focal depth of 23km for the 2008 mainshock with an uncertainty of  $\pm 5$ km.

Spatiotemporal analysis of post-Methoni seismic activity outlines 7 groups within panel F6F7 that characterize different parts of the activated region (Fig.4a, b). The distribution of the hypocenters jointly with their evolution in time and the part of the subduction system where these occur are



analytically discussed in the Appendix A. The constrained focal mechanisms (Fig.4c) and their P, T principal axes (Figure S1) also allow for several interesting observations and are hereafter jointly discussed.

## 5. Discussion

In this work, offshore seismicity has been constrained both horizontally and in depth by our dense local array of OBS stations, during a period between 9 and 21 months after the Methoni mainshock.

Despite its moderate magnitude in comparison to megathrust earthquakes in other subduction zones, the Methoni earthquake, is the largest interplate earthquake within the 400 km long western Hellenic subduction zone for over a half-century and was followed by post-seismic slip, as large as the coseismic slip, during the 3 year period after the mainshock. According to geodetic data modelling by Howell et al. (2017a), the afterslip area was twelve times larger than the coseismic patch, over a 100-km-wide segment spanning through the two panels F5-F6 and F6-F7, centered on the Methoni rupture (Fig.1b). The poorly constrained geodetic updip and downdip limits have been chosen to correspond to the forearc backstop trenchward edge and the 35 km depth respectively. The latter is roughly located below the Messenia and Mani capes.

Here we investigate the geometry and character of the post-Methoni seismicity within panel F6F7 (Fig.4a, b). We discuss it with respect to the shape and extension of the rupture area as well as the widely distributed post seismic deformation.

Two clusters (#6 in cyan and #7 in black) are located at depths above the updip and downdip edges of the rupture area, respectively (Fig.4b). Hypocenters extend through a 10 km thick layer above the interplate fault with only few events reaching shallower depths. These events have not been observed by our pre-Methoni offshore-onshore deployment, which is also the case for the other clusters discussed hereafter.

There is a complete lack of interplate activity between cluster #6 and #7 over a downdip width of about 30 km corresponding to the Methoni rupture area (Fig.4b and Fig.A.1b Profiles 1,2). It has been observed for many of the  $M > 8$  earthquakes such as Sumatra (Hsu et al., 2006), Chile (Hayes et al., 2014b; Li et al., 2016), and Tohoku (e.g Asano et al., 2011) that large co-seismic slip areas tend to

have little interplate seismicity after the mainshock rupture. The distribution of hypocenters, 9-21 months after the moderate  $M_w=6.8$  Methoni earthquake shows a similar feature. In addition, we observe that the surrounding deep upper plate volume, right above the plate interface is similarly quiet (Fig.4b).

There is a strong concentration of hypocenters along the slab fault F6 (Fig.4a, clusters #1 (red) and #2 (green)). Coseismic slip occurring on the megathrust fault plane which is here laterally bordered by a vertical fault zone located in the upward extent of the intraslab F6 fault, may induce earthquake swarms by micro-faulting. The present study area is located at shallower depths than the Moho of the overriding plate which is identified at  $\sim 30$  km depth beneath Messiniakos gulf (Sachpazi et al., 2016a). The overlying portion of the Aegean plate is thus largely crustal. The fact that the clusters #1 (red) and #2 (green) occur in the upper-plate crust (Fig.4b) within a vertical plane above the intra-slab fault F6, may highlight a process that triggers activity through fluid migration in a pre-stressed region above. Though, this activity is located downdip and not over the co-seismic area along the fault F6 due to post-seismic stress relaxation (see Fig. 5b Leonard and Stein, 2004) and/or due to lateral variation of fluids in the crustal material above the fault region. In fact, many causes might contribute to the observed spatio-temporal evolution.

The slab faults have already been shown to correlate with clustered seismicity, but this occurred at the 60-80 km slab depth within the subducting crust further downdip, beneath NE Peloponnesus and have been proposed to channel slab dehydrating fluids (Sachpazi et al., 2016a). Recent results, focusing on Greece but extended also to other subduction zones, proposed that fluids may migrate along the slab further updip and upwards, towards the overriding crust to trigger upper plate seismicity ( $<40$ km depth) (Halpaap et al., 2019). Our spatio-temporal analysis has shown that the shallower cluster along the fault F6 (cluster #1, red) precedes the deeper one (cluster #2, green) (Fig.A.1a), thus the fore-mentioned mechanism looks unlikely for our observations. Yet, it is possible that dehydration occurs locally at depth and that the deeper cluster is diagnostic of the upwards channelling of fluids.

Landwards, geodetic modelling is better constrained by the GPS stations and shows significant afterslip (Howell et al., 2017a) (Fig.1b). This is where seismicity downdip of the coseismic rupture (group #7, cluster in black) is located right above and on top of the plate interface (Fig.4b). This is

still located in the crust-to crust contact and the interplate is not yet under the mantle of the upper plate. So we can think of these aftershocks as essentially being driven by brittle creep as proposed by Perfettini & Avouac (2004) for deep afterslip. Alternatively, slow slip may similarly occur in the downdip part of the slab fault F6 to explain the earthquake clustering and induced deformation within the upper plate (clusters #1, #2). This would be due to the differential motion between the slab panels along this fault.

*Focal mechanisms and the nature of seismic deformation with respect to the plate interface*

Cluster #6 (cyan), located updip of the rupture area and just above the interplate boundary, is related with reverse and strike slip events (20-23km depth) with a P axis striking NE-SW (Fig. 4c and Fig. S1), consistent with the mainshock and major aftershocks (Fig. 2a). Cluster #5 (orange), located instead beneath the rupture area and within the subducting crust (Fig. 4b) contains normal-faulting events with a T-axis trending between N-S and NE-SW (2.6-50km depth) (Fig. 4c and Figure S1). This type of faulting is also observed in events located at the same depths in the nearby region of panel F7F8 with a T-axis trending roughly WE (Fig. 4c).

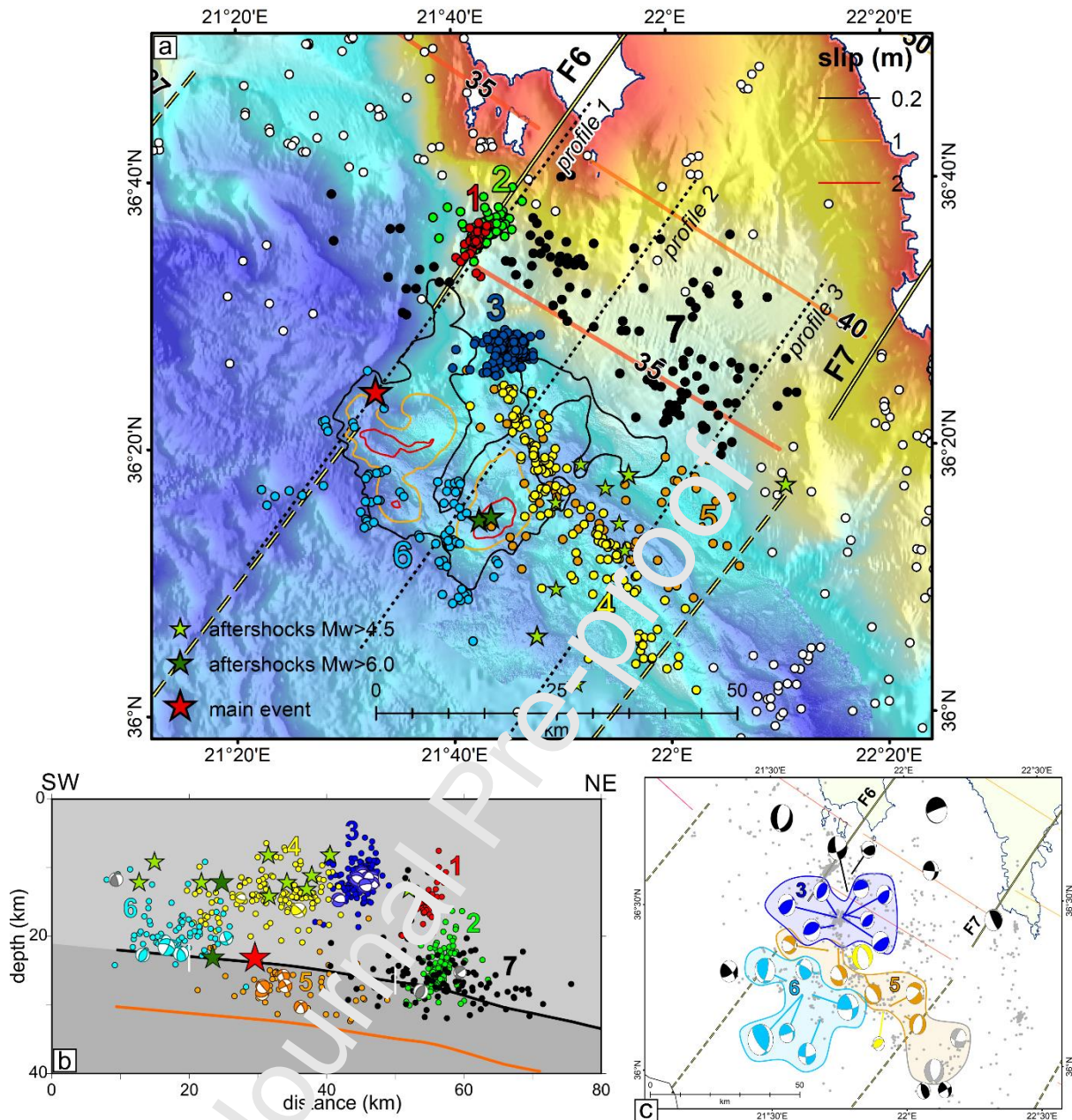


Fig. 4. (a) Seismicity of panel F6F7 with relocated epicenters using the double-difference method. Colours and numerical labels correspond to the 7 spatial groups discussed in the main text and Appendix A. Methoni coseismic slip is superposed. Profiles 1-3 (black dotted lines), drawn in a N35°E direction are used for the cross-sections of figure A.1.b. (b) Cross-section of the relocated seismicity in a N35°E direction covering the whole width of panel F6F7. Beachballs present the far-hemisphere projections of selected focal mechanisms, with their compressive quadrants following the same colour-coding as the hypocenters of the respective 7 spatial groups except for those with gray colour which do not belong to them. Hypocenters locations of the Methoni mainshock (red star) and

stronger aftershocks (green stars) of the first period (Fig.2b) are from the present study. Areas with light and dark gray shading represent the upper and lower plate, respectively. The bold black line shows the plate interface with the two white vertical ticks denoting the 30-km-long downdip mainshock rupture width along the western part of the panel. The bold orange line is the slab Moho assuming an 8km thick oceanic crust (Gesret et al., 2010) (c) Focal mechanisms for events within panel F6F7 and its vicinity. Beachballs with black and grey compressive quadrants correspond to events at depths related to the upper and lower plate, respectively.

In the offshore domain between the southwest Peloponnese and Crete, focal mechanisms of the most significant earthquakes in the last 40 years show that the regional stress field corresponds to two types of faulting. The first, reverse and low-angle thrust faulting with a NE horizontal compressive axis, has been considered to reflect the SW overriding of the Aegean domain over the Ionian oceanic crust causing also the large inter-plate subduction earthquakes (Shaw and Jackson, 2010; Benetatos et al., 2004; Kapetanidis and Kassaras, 2019). The second, reverse faulting within the lower plate with a trench parallel compressive axis is proposed to correspond to along-arc shortening of the subducted slab (Shaw and Jackson, 2010).

However, at the NW part of the subduction, in the Ionian Islands, small normal-fault earthquakes with a W-E trending T-axis have been resolved at shallow depths within the slab crust, by an early OBS and land-based network (Tschapazi et al., 2000). These events found trenchward of a change in the dip of the interplate boundary (Hirn et al., 1996), were interpreted as reflecting the bending of the lower plate. These types of events have also been found along the Japan trench and similarly attributed to bending-related faulting of the subducting crust (Gamage et al., 2009). In the Ionian islands, in addition to the lower plate extensional earthquakes, reverse-faulting events have been located in the upper plate above the interplate boundary, exhibiting a NE striking P-axis. The contrasting focal mechanisms on either side of the seismically imaged megathrust boundary -at 15km depth- were evidence it was the plate interface. We suggested that lower plate bending was due to the load of the southwestwards overriding upper plate which thickens landwards.



Our findings in the present study of the southwestern part of the subduction zone are consistent with these characteristics of background seismicity of the Ionian Islands. The normal fault earthquakes are in the lower plate crust and trenchwards of the thickened Hellenic continental margin and may mark the lower plate bending to underthrust the southwestwards advancing upper plate (Le Pichon et al., 2019). The plate interface may be thus defined as the boundary (at the 24-25km depth range) between the two groups of different focal mechanisms, with those around 20-23 km depth being at the base of the overriding upper plate, consistently with the proposed Methoni mainshock's hypocenter at 23km depth.

#### *Seismic activity within the shallow upper plate*

The third group (cluster #3, blue) in the shallower part of the upper plate is located 10 km above the plate interface and above the downdip coseismic border region (Fig.4b). It displays reverse faulting events with an along-arc P-axis (Fig.4c and Figure S1) that differs significantly from the regional NE striking horizontal compressive axis. It is possible that this seismic swarm in the hanging wall, which occurred 13 months after the mainshock, is associated with Coulomb stress transfer above the lateral variation of rupture imposed on an obliquely orientated structure (Vallage et al., 2014).

Cluster #4 (yellow) exhibits a tight geographical association with the Matapan Trough. Such relation has already been noted during the pre-Methoni period, in the wider offshore forearc, though MT associated activity was not continuing into panel F6F7 (Fig.3b). During the post-Methoni period, MT is seismically active at the 10-15 km depths range into panel F6F7. This suggests the presence of deep active faults controlling its morphological expression at the sea bottom within the outer forearc crust, which have been seismically activated in the post-Methoni period (Fig.3a). The focal mechanisms we could constrain for two events at 15 km depth beneath MT (panel F7F8) display reverse and strike slip faulting respectively with a NE trending P-axis (Fig.4c and Figure S1). The extensional process that was suggested for the formation of this deep outer forearc domain (Lallemant et al., 1994) is possibly currently replaced by oblique compression. This might result from the combined effect of the ongoing collision between the backstop and the Lybian margin south of Crete, as suggested by Mascle and Chaumillon (1998), and from the predicted ~2cm/yr of dextral motion at the trenchward backstop's edge as suggested by Chamot-Rooke et al. (2005).



*What drives post-Methoni seismicity*

We document a seismic activation of the upper plate which appears to accommodate deformation on small faults with different orientations around and above the area of mainshock slip. We attribute this activation to a part of the post-seismic deformation which spreads induced elastic deformation into the forearc hanging wall of the interplate fault. Howell et al., 2017a model the 20mm post seismic displacement as mainly related to widespread aseismic slip of the plate interface. It is beyond the scope of this paper to interpret GPS data but we note a change in the slope of geodetic offset (see time series of stations METH and KERY at Fig.4b of Howell et al., 2017a and panel in Fig.2b) at the end of 2008. Most of the ~15mm post seismic displacement occurs before the end of 2008 and the remaining ~5mm continue up to the end of 2010. The onset of slow deformation coincides in time with the initiation of the smaller clustered activity during our post-Methoni experiment (Fig.2b). The earlier large aftershocks which also occurred in the shallow upper plate took place during the first period of faster rate deformation (Fig.2b). Their focal mechanisms, strike slip as well as reverse faulting, are compatible with upper plate deformation, also shown in the kinematics of the co-seismic slip, which is driven by the SW movement of the overlying plate.

We also resolve the eastern part of panel F6F7 which did not slip coseismically, to be devoid of interplate activity in the 30km along-dip range (Fig.A.1b Profile 3). The  $M_w=6.8$  main shock was followed 2 hours later by the  $M_w=6.5$  interplate aftershock at the southeastern border of the Methoni asperity which may have continued the rupture in some extent to the SE, towards slab fault F7 (Sachpazi et al., 2016b). Unfortunately available data are insufficient to model its co-seismic slip; hence its along-dip extent is unknown. Thus, we cannot exclude the possibility that a part of the silent plate interface of the eastern panel has experienced aseismic slip as proposed by Howell et al., 2017a.

During our pre-Methoni experiment period the whole western part of the panel was shown to be seismically quiet in comparison to the eastern one (Fig.3b), which may also be observed in the several years back, -though less well resolved- NOA seismicity (FigureS2). NOA epicentral locations following our post-Methoni experiment (2010-2019) show a progressive decrease in seismic activity- also along the wider forearc- and approach to the pre-Methoni state (Fig.S3 panel F6F7). Over the Methoni coseismic domain, this may suggest progressive relocking of the asperity and strong coupling

between the plates (Sachpazi et al., 2016b). The persistence of MT related seismic activity, -outside panel F6F7- during our short-term pre- and post-Methoni experiments suggests a difference in the seismic behavior along the forearc. It is possible that the same processes we proposed to drive post-seismic deformation of panel F6F7, such as dehydration-embrittlement and/or aseismic slip, are behind the continuous MT related seismic activity. Clarifying the processes at work will require sea-bottom geodetic and seismic monitoring.

We have shown that the clustered post-Methoni seismic activity within the outer forearc crust on the one hand and the localized slip during the Methoni earthquake along the plate interface on the other hand, accommodate complementary patterns of the seismic deformation, over the megathrust boundary. Oblique convergence structures were up to now considered to be restrained at the trenchward backstop's edge (Chamot Rooke et al., 2005), and the Methoni sequence documents a potentially active oblique deformation up to the Matapan Trough. Our findings, on the Methoni sequence document in detail the characteristics of this part of the SW Hellenic subduction zone with a highly deformable Aegean plate overriding a segmented lower plate.

## 6. Conclusions

The results of our long-term aftershocks study of the Methoni Mw 6.8 interplate event, acquired from recordings of both OBS and land stations, provide insights into the SW Hellenic megathrust domain where large events are uncommon, though a large historical tsunamogenic event has occurred in the past (Papazachos and Papazachou, 2003; Stiros and Papageorgiou, 2001). We establish spatial correlation between the regional seismicity pattern and the Matapan Trough, a major -250-km-long forearc basin within our study area, already identified by our previous studies with less dense datasets (Sachpazi et al., 2016b). We discuss spatio-temporal variations of the long-term aftershocks activity, which clustered over the Methoni co-seismic and post-seismic slip area thanks to depth constraints and focal mechanisms.

We showcase clear evidences of post-Methoni crustal seismicity occurring on mega-thrust asperities and forearc crust's faults, as well as the impact of the slab segmentation (slab fault F6) in the spatial distribution. These features did not show up before the 2008 Methoni earthquake as

documented by comparison with pre-Methoni seismic studies (Sachpazi et al., 2016b). Though the largest crustal aftershocks account for only a small fraction of the moment release and post-seismic slip documented by GPS data (Howell et al., 2017a), our results indicate that the observed post-Methoni microseismic activity is consistent with complementary post-seismic slow deformation which spreads into the forearc region rather than on the plate interface.

### Acknowledgments

This research has been supported by the European Union FP6 NEXT INSIGHT program, under the project THALES WAS RIGHT. We thank the editor and two anonymous reviewers for their critical evaluation.

### References

- Asano, Y., Saito, T., Ito, Y., Shiomi, K., Hirose, H., Matsumoto, T., Aoi, S., Hori, S., Sekiguchi, S., 2011. Spatial distribution and focal mechanisms of aftershocks of the 2011 off the Pacific coast of Tohoku earthquake. *Earth Planet. and Space* 63, 669–673. doi:10.5047/eps.2011.06.016.
- Baker, C., Hatzfeld, D., Lyon-Caen, H., Papadimitriou, E., Rigo, A., 1997. Earthquake mechanisms of the Adriatic Sea and Western Greece: geodynamic implications for the oceanic subduction-continental collision transition. *Geophys. J. Int.* 131, 559-594.
- Benetatos, C., Kiratzi, A., Papazachos, C., Karakaisis, G., 2004. Focal mechanisms of shallow and intermediate depth earthquakes along the Hellenic Arc. *C. Journal of Geodynamics*, 37, 253–296.
- Brosolo, L., Mascle, J., Loubtrieu, B., 2012. Morpho-Bathymetry of the Mediterranean Sea, Map 1/4.000.000, 1st ed., Comm. for the Geol. Map of the World (CGMW) and UNESCO, Paris.
- Cattania, C., Hainzl, S., Wang, L., Enescu, B., Roth, F., 2015. Aftershock triggering by postseismic stresses: A study based on Coulomb rate-and-state models. *J. Geophys. Res., Solid Earth*, 120, 2388–2407. doi:10.1002/2014JB011500.

- Chamot Rouke, N., Rabaute, A., Kreemer, C., 2005. Western Mediterranean Ridge mud belt correlates with active shear strain at the prism-backstop geological contact. *Geology* 33(11), 861–864. [doi:10.1130/G21469](https://doi.org/10.1130/G21469).
- Chatelain, J.L., 1978. Etude fine de la sismicite en zone de collision continentale au moyen d'un r'eseau de stations portables: la regionHindu-Kush Pamir, These de 3eme cycle, Universite de Grenoble, 219 pp.
- Chaumillon, E., Mascle, J., Hoffmann, H.J., 1996. Deformation of the western Mediterranean Ridge: Importance of Messinian evaporitic formations. *Tectonophysics* 263, 163-190.
- England, P., Houseman, G., Nocquet, J.M. 2016. Constraints from GPS measurements on the dynamics of deformation in Anatolia and the Aegean. *J. Geophys. Res.: Solid Earth*, 121: 8888–8916, [doi:10.1002/2016JB013382](https://doi.org/10.1002/2016JB013382).
- Gamage, S.S.N., Umino, N., Hasegawa, A., Kirby, S.H., 2009. Offshore double-planed shallow seismic zone in the NE Japan forearc region revealed by sP depth phases recorded by regional networks. *Geophys. J. Int.* 178, 195–214.
- Gesret, A., Laigle, M., Diaz, J., Sachpazi, M., Hirn, A., 2010. The oceanic nature of the African slab subducted under Peloponnesus: Thin layer resolution from multiscale analysis of teleseismic P to S converted waves. *Geophys. J. Int.* 183, 833–849. [doi:10.1111/j.1365-246X.2010.04738.x](https://doi.org/10.1111/j.1365-246X.2010.04738.x).
- Halpaap, F., Rondenav, S., Perrin, A., Goes, S., Ottemoller, L., Austrheim, H., Shaw, R., Eeken T., 2019. Earthquakes track subduction fluids from slab source to mantle wedge sink. *Sci. Adv.* 5(4), eaav7369.
- Hayes, G.P., Furlong, K.P., Benz, H.M., Herman, M.W., 2014a. Triggered aseismic slip adjacent to the 6 February 2013 *M*W 8.0 Santa Cruz Islands megathrust earthquake. *Earth Planet. Sci. Lett.* 388, 265–272. [doi:10.1016/j.epsl.2013.11.010](https://doi.org/10.1016/j.epsl.2013.11.010).
- Hayes, G.P., Herman, M.W., Barnhart, W.D., Furlong, K.P., Riquelme, S., Benz, H.M., Bergman, E., Barrientos, S., Earle, P.S., Samsonov, S., 2014b. Continuing megathrust earthquake potential in Chile after the 2014 Iquique earthquake. *Nature* 512, 295–298. [doi:10.1038/nature13677](https://doi.org/10.1038/nature13677).

- Hirn, A., Sachpazi, M., Siliqi, R., Mc Bride, S., Marnelis, F. and the STREAMERS/PROFILES group, 1996. A traverse front with coincident normal incidence and wide angle seismic. *Tectonophysics* 267, 57-71.
- Howell, A., Palamartchouk, K., Papanikolaou, X., Paradissis, D., Raptakis, C., Copley, A., England, P., Jackson, J., 2017a. The 2008 Methoni earthquake sequence: the relationship between the earthquake cycle on the subduction interface and coastal uplift in SW Greece. *Geophys. J. Int.* 208, 1592–1610.
- Hsu, Y.J., Simons, M., Avouac, J.P., Galetzka, J., Sieh, K., Chlieh, M., Natawidjaja, D., Prawirodirdjo, L., Bock, Y., 2006. Frictional afterslip following the 2005 Nias-Simeulue earthquake, Sumatra. *Science* 312, 1921–1926. *doi:10.1126/science.1126960*.
- Huchon, P., Lyberis, N., Angelier, J., Le Pichon, X., Feraud, V., 1982. Tectonics of the Hellenic trench: a synthesis of Seabeam and submersible observations. *Tectonophysics* 86, 69-112.
- Hussni, S., Becel, A., Schenini, L., Laigle, M., Dessu, J.X., Galve, A., Vitard, A., SISMED Scientific Team. 2017. Pre-Stack depth Migration imaging of the Hellenic Subduction Zone. POSTER SESSION AGU FALL MEETING.
- Jongsma, D., 1977. Bathymetry and shallow structure of the Pliny and Strabo Trenches south of the Hellenic Arc. *Geol. Soc. Am. Bull.* 88, 797–805.
- Jackson, J., McKenzie, D., 1988. The relationship between plate motions and seismic moment tensors, and the rates of active deformation in the Mediterranean and Middle East. *Geophys. J. R. Astr. Soc.* 93, 45-73.
- Jackson, J., McKenzie, D., 1988. Rates of active deformation in the Aegean Sea and surrounding regions, *Basin Res.* 1, 121-128.
- Kahle, H. G., Cocard, M., Peter, Y., Geiger, A., Reilinger, R., Barka, A., Veis, G., 2000. GPS-derived strain rate field within the boundary zones of the Eurasian, African, and Arabian plates, *J. Geophys. Res.* 105, 23,353–23,370. *doi:10.1029/2000JB900238*.

- Kapetanidis, V., Kassaras, I., 2019. Contemporary crustal stress of the Greek region deduced from earthquake focal mechanisms. *J. of Geodynamics* 123, 55–82.
- Kissling, E., 1995. Program VELEST user's guide - short introduction, Institute of Geophysics, ETH Zurich.
- Kissling, E., Ellsworth, W.L., Eberhart-Phillips, D., Kradolfer, U., 1994. Initial reference models in local earthquake tomography. *J. Geophys. Res.* 99, 19635–19646. *doi:10.1029/93JB03138*.
- Laigle, M., Sachpazi, M. Hirn, A., 2004. Variation of seismic coupling with slab detachment - upper plate structure along western Hellenic subduction. *Tectonophysics* 391, 85-95.
- Lallemant, S., Truffert, C., Jolivet, L., Henry, P., Chamot-Rooke, N. de Voogd, B., 1994. Spatial transition from compression to extension in the Western Mediterranean Ridge accretionary complex. *Tectonophysics* 234, 33–52.
- Lee, W.H.K., Valdes, C.M., 1989. User manual for HYPO7PC, in Lee, W.H.K., ed., Toolkit for seismic data acquisition, processing and analysis: El Cerrito, Calif. Seismological Society of America, International Association of Seismology and Physics of the Earth's Interior Software Library, v. 1, p. 203-236.
- Li, L., Lay, T., Cheung, K.F., Ye, L., 2016. Joint modeling of teleseismic and tsunami wave observations to constrain the 16 September 2015 Illapel, Chile, *MW* 8.3 earthquake rupture process. *Geophys. Res. Lett.* v. 43, p. 4305–4312. *doi:10.1002/2016GL068674*.
- Lin, J., Stein, R. S., 2004. Stress triggering in thrust and subduction earthquakes and stress interaction between the southern San Andreas and nearby thrust and strike-slip faults. *J. Geophys. Res.* 109, B02303. *doi:10.1029/2003JB002607*.
- Le Pichon, X., Angelier, J., Sibuet, J.-C., 1982. Plate boundaries and extensional tectonics. *Tectonophysics* 81, 239-256.
- Le Pichon, X., Lallemant, S., 2002. The Mediterranean Ridge backstop and the Hellenic nappes. *Marine geology* 186,111-125.
- Le Pichon, X., Sengor, C.A.M., Imren, C., 2019. A new approach to the opening of the Eastern Mediterranean Sea and the origin of the Hellenic Subduction Zone. Part 2 The Hellenic Subduction. *Can. J. Earth Sci.* 56, 1144-1162.



- Mascle, J. Chaumillon, E., 1998. An overview of Mediterranean Ridge collisional accretionary complex as deduced from multichannel seismic data. *Geo-Mar. Lett.* 18, 81-89.
- Meier, T., Rische, M., Endrun, B., Vafidis, A. Harjes, H. P., 2004a. Seismicity of the Hellenic subduction zone in the area of western and central Crete observed by temporary local seismic networks, *Tectonophysics* 383(3), 149-169.
- Nocquet, J. M., 2012 Present Day kinematics of the Mediterranean: A comprehensive overview of GPS results. *Tectonophysics* doi:10.1016/j.tecto.2012.03.037.
- North, R.G., 1974. Seismic slip rates in the Mediterranean and Middle East. *Nature* 252, 560-563.
- Ozawa, S., Nishimura, T., Munekane, H., Suito, H., Kobayashi, C., Tobita, M., Imakiire, T., 2012. Preceding, coseismic, and postseismic slips of the 2011 Tohoku earthquake, Japan: *J. Geophys. Res.* 117 B07404. doi:10.1029/2011JB009120.
- Papazachos, B. C., Papazachou, K., 2003. *The Earthquakes of Greece*, 286 pp., Ziti Publ., Thessaloniki.
- Perfettini, H., Avouac, J.-P., 2004. Postseismic relaxation driven by brittle creep: A possible mechanism to reconcile geodetic measurements and the decay rate of aftershocks, application to the Chi-Chi earthquake, Taiwan. *J. Geophys. Res.* 109, B02304. doi:10.1029/2003JB002488.
- Reilinger, R., McClusky, S., Parolisi, D., Ergintav, S., Vernant, P., 2010. Geodetic constraints on the tectonic evolution of the Aegean region and strain accumulation along the Hellenic subduction zone. *Tectonophysics* 488, 22-30.
- Reston, T. J., von Huene, K., Dickmann, T., Klaeschen, D., Kopp, H., 2002b. Frontal accretion along the western Mediterranean Ridge: the effect of Messinian evaporites on wedge mechanics and structural style. *Marine geology* 186(1), 59-82.
- Roumelioti, Z., Benetatos, C., Kiratzi, A., 2009. The 14 February 2008 earthquake (M6.7) sequence offshore south Peloponnese (Greece): Source models of the three strongest events. *Tectonophysics* 471, 272-284. doi:10.1016/j.tecto.2009.02.028.

- Sachpazi, M., Hirn, A., Clément, C., Haslinger, F., Laigle, M., Kissling, E., Charvis, P., Hello, Y., Lépine, J.C., Sapin, M., Ansorge, J. 2000. Western Hellenic subduction and Cephalonia transform: local earthquakes and plate transport and strain. *Tectonophysics* 319, 301-319.
- Sachpazi, M., Laigle, M., Charalampakis, M., Diaz, J., Kissling, E., Gesret, A., Becel, A., Flueh, E., Miles, P., Hirn, A., 2016a. Segmented Hellenic slab rollback driving Aegean deformation and seismicity. *Geophys. Res. Lett.* 43, 651–658. doi:10.1002/2015GL066818.
- Sachpazi M., Laigle, M., Charalampakis, M., Sakellariou, D., Flueh, E., Sokos, E., Daskalaki, E., Galvé, A., Petrou, P., Hirn, A., 2016b. Slab segmentation controls the interplate slip motion in the SW Hellenic subduction: New insight from the 2008 Mw 6.8 Methoni interplate earthquake. *Geophys. Res. Lett.* 43, 9619–9626.
- Shaw, B. *et al.*, 2008. Eastern Mediterranean tectonics and tsunami hazard inferred from the AD 365 earthquake, *Nat. Geosci.* 1(4), 268–276.
- Shaw, B., Jackson, J., 2010. Earthquake mechanism and active tectonics of the Hellenic subduction zone. *Geophys. J. Int.* 181, 966–984. doi:10.1111/j.1365-246X.2010.04551.x.
- Stiros, S.C., Papageorgiou, S., 2001. Seismicity of Western Crete and the destruction of the town of Kisamos at AD 365: archaeological evidence. *J. Seismol.* 5, 381–397.
- Vallage, A., Deves, M. H., Klingenberg, Y., King, G. C. P., Ruppert, N. A., 2014. Localized slip and distributed deformation in oblique settings: the example of the Denali fault system, Alaska. *Geophys. J. Int.* doi:10.1093/gji/ggu.00.
- Vernant, P., Reilinger, R., McClusky, S., 2014. Geodetic evidence for low coupling on the Hellenic subduction plate interface. *Earth Planet. Sci. Lett.* 385, 122–129. doi:10.1016/j.epsl.2013.10.018.
- Vitard, C., Charvis P., Laigle M., Sachpazi M., Galve A., Schenini L., Dannowski A., Spyridon B., 2015. Structural analysis of the southwestern segment of the Hellenic subduction zone by joint analysis of seismic reflection and refraction. *Poster*, Fall Meeting, AGU, San Francisco, Calif.
- Yagi, Y., Kikuchi, M., Nishimura, T., 2003. Co-seismic slip, post-seismic slip, and largest aftershock associated with the 1994 Sanriku-haruka-oki, Japan, earthquake. *Geophys. Res. Lett.* 30, 2177. doi:10.1029/2003GL018189.

**APPENDIX A***Spatiotemporal analysis of the 2008-2009 Methoni seismicity*

To enable the spatiotemporal analysis of the Methoni earthquake sequence during the study period, we applied a spatial grouping methodology similar to the one followed for the relocation procedure to the final catalogue which is fully described in the Supplementary Material. Particular focus was placed in the clustered seismicity that has occurred within panel F6F7 and especially on slab fault F6, while the rest of activity in the other panels or further onshore is considered here as a “background seismicity”. An inter-event distance matrix was constructed for the focused seismicity and Ward’s (1963) linkage was applied to create hierarchical clustering. By selecting proper thresholds, the seismicity was initially divided in several spatial groups, which were then adjusted, merged and reduced to a selection of 7 groups that characterize different parts of the activated region within panel F6F7 (Fig.4a). Post-Methoni activity at the beginning of the experiment (mid-October 2008), ~9 months after the mainshock (M) presented a relatively steady background rate of about 2-3 events per day (Fig.A.1a).

*Group #1 red (M+10 months)*

On 14 December, a sudden increase of activity was identified as group #1 (red). Epicentres were aligned along the trace of slab fault F6 beyond the downdip rupture area (Fig.4a), but at much shallower depths of 12-17 km, hence in the upper plate (Fig.A.1b Profile 1). This spatiotemporal cluster began with smaller events was then followed by a larger one ( $M_L=4.2$ ) and continued for 11 days.

*Group #2 green (M+11 months)*

On 15 January 2009, a different cluster (#2; green) was activated on slab fault F6 (Fig.4a), mostly in the overriding plate at depths of 20-28km (Fig. A.1b Profile 1). This cluster evolved into a series of small bursts including mainly a few  $M_L>3.0$  events, with the larger being an  $M_L=3.5$  event (Fig. A.1a). Most of its activity was over by mid-February 2009. Although cluster #2 is located close to #1, both being downdip of the northwestern coseismic slip patch extent (Fig.4a), they are well-separated in both space and time and have occurred at distinctly different depths. Both are located in the upper plate while the second one extends downward to reach the plate interface. They both present an

apparently sub-vertical distribution; however, no clear direction of migration in depth with time could be identified within each individual cluster. By the end of the second cluster's occurrence, both groups #1 and #2 cover a column at depths 10-30km aligned horizontally along the fault system F6, in an almost linear 5-km-long segment oriented SW-NE (Fig.A.1b Profile 1). Although there is a partial overlap between their epicenters, cluster #1 appears to have occurred at the NW half of the activated zone while cluster #2 mainly occupies the SE half.

*Group #3 blue (M+13 months)*

Cluster #3 (blue) was initiated with an  $M_L=3.5$  event on 28 March 2009, followed by a few events during the next day (Fig.A.1a). A new burst of its activity was triggered by a couple of  $M_L=3.9-4.0$  events on 5 April, with a rate of 2-3 events/day for the next 25 days. A stronger outbreak began on 23 May 2009, following an  $M_L=3.8$  event, starting with a rate of 25 events/day which slowly diminished, but the cluster remained active until the end of the study period, in September 2009. Due to the comparable magnitudes between the largest event of this cluster, it can be characterized as a swarm. Located ~16km SSE of clusters #1 and #2, and ~10km SE of the slab fault F6, it fills the geographical gap between the two main patches that ruptured during the 2008 Methoni mainshock (Fig.4a). This group occurs within the overriding plate, mainly at depths between 10 and 15 km (Fig. A.1b Profile 2).

The other spatial groups within panel F6F7 do not present any significant spatiotemporal clustering, but are composed of diffuse seismicity that generally delineates different regions of particular interest.

*Group #4 yellow*

Spatial group #4 (yellow), covers a roughly linear region along ~50km SSE of cluster #3, reaching slab fault F7 (Fig.4a). It is located at the borders of the higher slip area of the 2008 main rupture and relates geographically with the MT region across the whole panel (Fig.4a). This area includes almost all the largest aftershocks of the first period before our post-Methoni experiment (Fig.2a). It is distributed at depths between 10 and 20km, but is mostly concentrated at 14-15km, thus confined in the upper plate (Fig. A.1b Profiles 2 and 3). Its evolution in time exhibits an almost constant rate of 0.3-0.4 events/day with the exception of a small burst (10-17 April) including three  $M_L=3.5$  events (Fig. A.1a).

*Group #5 orange*

Spatial group #5 (orange) covers a 35km x 15km region of diffuse seismicity constrained at depths of 25-30km (Fig. A.1b profiles 2,3), which corresponds to the lower plate oceanic crust. It presents a very low seismicity rate of 0.1-0.2 events/day throughout the study period (Fig. A.1a).

*Group #6 cyan*

Spatial group #6 (cyan) is located updip of the Methoni rupture, at the western part of the panel (Fig.4a). Though dispersed, it clearly follows the edges of the updip extent of the coseismic slip area, with focal depths mainly in the range 17-23km, mostly concentrated at 20km depth (Fig. A.1b profiles 1,2 at distances 40-50km along the X axis) hence right above the interplate boundary. Despite its low background rate, it also contains the strongest event of the study period, an  $M_L=4.4$  earthquake that occurred on 21 April 2009 and caused a short outburst of ~20 events during the following 10 days, including an  $M_L=4.0$  event on 27 April 2009 (Fig. A.1a). This episode took place half-way through the first period of activity at cluster #3.

*Group #7 black*

Lastly, spatial group #7 (black) is located further NE, across-panel F6F7 in a NW-SE direction reaching slab fault F6 at about the same place as clusters #1 and #2, with its focal depths being distributed in the range 23-30km (Fig. A.1b, profiles 1-3). This group does not present any significant bursts of activity, but rather a constant seismicity rate of ~0.2 events/day which appears to slightly increase to 0.5 events/day after the initiation of cluster #3 in April 2009 (Fig. A.1a).

Besides the activity in panel F6F7, the rest of the study area (background seismicity) contains hypocenters spreading in a wide depth range (10-30km) (Fig.3a) and exhibits a seismicity rate of 1-2 events/day. Beneath Matapan Trough (MT), the hypocenters are mainly located in the upper plate apart from those along panel F6F7 and its vicinity for which also the lower plate presents some activity (Fig. A.1c). Hypocentral distribution along MT from our 1-year-long experiment, shows no detectable shallow seismic activity (<10km depth) that would support the presence of a seismically active separate regional outcropping fault proposed by Shaw et al., 2010.

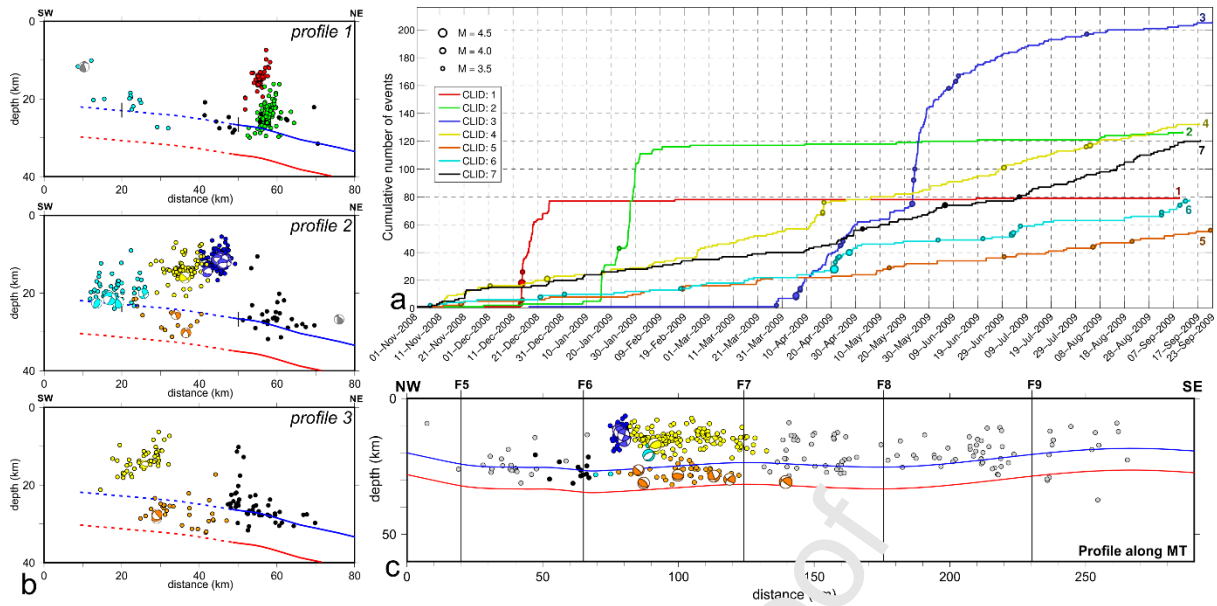


**Fig. A.1** Spatiotemporal analysis results and seismicity cross-section along the Matapan Trough. (a) Cumulative number of events per spatial group for the post-Methoni experiment in panel F6F7. Different colors correspond to the different spatial group, also represented by a cluster ID (1-7) similarly to Fig.4a. The larger events ( $M > 3.5$ ), are marked with circles, with their size being proportional to the magnitude (b) Cross-sections of the clustered relocated hypocenters within panel F6F7, (top) profile 1: along slab fault F6, (middle) profile 2: central part and (bottom) profile 3: eastern part of panel F6F7. The two black vertical ticks on the blue lines of panel (b) at horizontal distances of 20 and 50 km are denoting the 30-km-dip mainshock rupture width along the western part of panel F6F7 (see also Fig. 4b). Beachballs present the far-hemisphere projections of selected focal mechanisms, with their compressive quadrants following the same colour-coding as the hypocenters of the respective spatial groups. (c) 20km-wide cross-section of relocated hypocenters projected along the MT (black dashed NW-SE-trending line in Fig.3a). The continuous vertical lines denote the location of the slab faults from Sachpazi et al., 2016b). Blue and red solid lines in panels (b) and (c) are for the top and base of the lower plate crust proposed by RF imaging (Sachpazi et al., 2016b), while the respective dashed lines (panel b) represent their updip prolongation, proposed by this study, assuming an 8km thick oceanic crust (Gesret et al., 2010). The plate interface depth southeastwards of slab fault F8 is obtained from a recently acquired seismic profile west of Crete (Hussni et al., 2017).



Journal Pre-proof

M.S. wrote the basis of the submitted paper, V.K. processed and analysed the data and also contributed to the interpretation of the results, M.C. contributed to the interpretation of results and developed the presentation and artwork from data, A.F. and E.D. processed and analysed the data, M.L., E.K., E.F. and A.H. contributed to the interpretation of the data, A.H., M.L. and M.S. coordinated the TWR project and contributed to the concept development.

Journal Pre-proof

### Highlights

- Spatio-temporal distribution of the Mw 6.8 Methoni aftershocks by OBS.
- Aftershocks driven by afterslip.
- Post-seismic deformation spread within the forearc crust.
- Bending-related normal faulting of the subducting crust.

Journal Pre-proof